PROCEEDINGS OF SCIENCE

# An intense positron source based on oriented crystals

**N. Canale,[a] P. Fedeli,[a,*] F. Alharthi,[b] I. Chaikovska,[b] R. Chehab[b] and L. Bandiera[a] for the e+BOOST collaboration [c]**

[a] *University of Ferrara, Department of Physics and Earth Sciences – INFN Ferrara, Via Saragat 1, 44122 Ferrara, Italy*

[b] *IJCLab, Université Paris-Saclay, Orsay, France*

[c] *The full collaboration list can be found in the Appendix.*

*E-mail:* ncanale@infn.fe.it, pierluigi.fedeli@infn.fe.it

The e+BOOST (intense positron source Based On Oriented crySTals) project investigates an innovative positron production scheme exploiting coherent radiation phenomena in oriented crystals. This technique offers a path toward the high-intensity positron beams required by future lepton colliders such as FCC-ee, CLIC, and CepC to achieve their luminosity goals. Traditional positron sources rely on high-energy electrons impinging on amorphous targets, a method limited by the Peak Energy Deposition Density (PEDD) and total energy deposited (Edep), both crucial parameters. For circular colliders like FCC-ee, PEDD is generally manageable in current designs; however, the total energy deposited still imposes significant constraints on the cooling and stability of the target. In linear colliders such as CLIC, both PEDD and Edep represent major limiting factors due to intense beam power and pulsed operation. By contrast, the use of oriented crystals enhances coherent radiation emission, improving $e^+e^-$ pair production efficiency while significantly reducing the total energy deposited in the converter material, easing thermal loads and extending target longevity. The proposed crystal-based concept adopts a hybrid target system: a thin oriented crystal radiator followed by a thicker amorphous converter. The radiator generates a high flux of photons, which the converter then transforms into $e^+e^-$ pairs. This configuration, first proposed and validated at CERN and KEK, is presently under study within the FCC-ee injector design framework. Recent experimental results confirm a significant increase in radiation yield when the crystal is accurately aligned with the incident beam. These measurements also validate the underlying simulation tools, which now guide the optimization of next-generation positron sources for FCC-ee. This work summarizes the recent achievements of the e+BOOST collaboration, including new experimental data and simulation studies advancing the design of efficient, high-intensity positron sources for future colliders.

*Speaker


ISSN 1824-8039. Published by SISSA Medialab.



PoS(EPS-HEP2025)584

## 1. Introduction

The European Strategy for Particle Physics provides clear guidance toward the realization of a new, high-performance accelerator to push beyond the energy frontier set by the LHC, enable more precise electroweak measurements, deepen our understanding of Higgs-boson couplings, and deliver strong discovery potential for new physics [1]. Among the proposed facilities, the FCC-ee [2] offers all the key capabilities to meet these ESPP objectives. The FCC-ee collider is designed to operate at four center-of-mass energy points: the Z pole, the $W^+W^-$ production threshold, the $ZH$ production peak, and the $t\bar{t}$ threshold. The first stage of the injector complex includes separate linacs for electrons and positrons up to a beam energy of 2.86 GeV [3] and must provide high-quality electron and positron sources to sustain the very high luminosity targeted by FCC-ee. Among the four operational modes of FCC-ee, the Z-pole is the most critical for the injector performance, strictly related to the positron source. In the conventional positron-source scheme, a primary electron beam impinges on a high-atomic-number amorphous target, typically tungsten, electrons interacting in the target generate bremsstrahlung photons, which subsequently convert into $e^+e^-$ pairs; the positrons are then captured and transported to the subsequent accelerator chain. Unfortunately, this conventional approach becomes unsustainable at high primary-beam intensities: ionization energy deposition in the target leads to excessive heating and material damage, while the non-uniform Peak Energy Deposition Density (PEDD) produces steep temperature gradients that induce thermal stresses, ultimately causing target degradation and failure. Experimentally, a damage threshold of about 35 J/g was established for amorphous tungsten targets at the SLC [4]. Within the CHART collaboration, dedicated studies on the FCC-ee injector are actively progressing [5], and a promising avenue is the use of oriented crystals in the positron-source scheme.

When a crystal is aligned so that a high-energy charged particle traverses close to a major crystallographic plane or axis, the Coulomb fields of lattice nuclei and electrons can be replaced by the continuum potential averaged along the plane or axis. In this regime, coherent effects emerge that modify the standard Bethe–Heitler description of electromagnetic interactions. Two coherent mechanisms enhance the photon spectrum relative to ordinary Bremsstrahlung [6–10]. The first is *channeling radiation* (CR), which occurs when the incidence angle lies within the Lindhard critical angle,

$$\theta_L \simeq \sqrt{\frac{2U_0}{\varepsilon}}, \tag{1}$$

where $U_0$ is the depth of the planar/axial continuous potential and $\varepsilon \approx pv$ denotes the particle energy in the ultrarelativistic limit. Under channeling, negatively charged particles are repelled from the atomic strings/planes and oscillate within the inter-planar (or axial) potential well, whereas positively charged particles are attracted and oscillate near the planes/strings; the associated transverse oscillations give rise to CR. The second mechanism is *coherent Bremsstrahlung* (CB), an over-barrier process that arises when the transverse momentum transfer matches the reciprocal-lattice vector. The resulting emitted radiation features constructive interference producing narrow, intense spectral and angular peaks whose characteristic frequencies are set by the crystal periodicity, leading to a photon spectrum that is more intense than in amorphous targets [9, 11]. Consequently, the production of a more intense radiation, upon pair conversion, yields a higher number of positrons per primary electron, thereby improving source efficiency and easing target-load constraints.

## 2. Crystal-based positron sources: experimental and simulation studies

Intense positron production can be achieved by exploiting coherent radiation effects in oriented crystals. Axial alignment in high-$Z$ materials is typically preferred due to the presence of strong electromagnetic fields and a favorable photon spectrum extending into the GeV range [12–14]. Most photons produced in this regime convert into positrons below approximately 100 MeV, thereby enhancing the capture efficiency in downstream optics [15]. The effective axial acceptance is typically on the order of a few milliradians.

Studies for future collider applications advocate a *hybrid* layout which was proposed for the first time in 1989 [12, 14] and validated at CERN in 2002 [16] and at KEK in 2003 [17, 18]. The hybrid layout consist of a thin ($< 1X_0$) crystal radiator, where $X_0$ the radiation length as defined in [19], followed by an amorphous converter (Fig. 1. c) [20–22]. In this configuration, the energy deposition is distributed between two elements: the crystal radiator, which remains below the shower-initiation thickness, while the naturally diverging photon beam spreads the energy load in the converter, thereby reducing PEDD while maintaining a high positron yield [22]. A single thicker oriented crystal (Fig. 1. b) provides a more compact design, though it introduces greater thermal challenges, such a design remains promising for moderate-intensity applications, such as FCC-ee [21]. In case of high-intensity linear colliders one can optimize the hybrid systems incorporating beam collimation or magnetic sweeping (Fig. 1. d,e) [22].

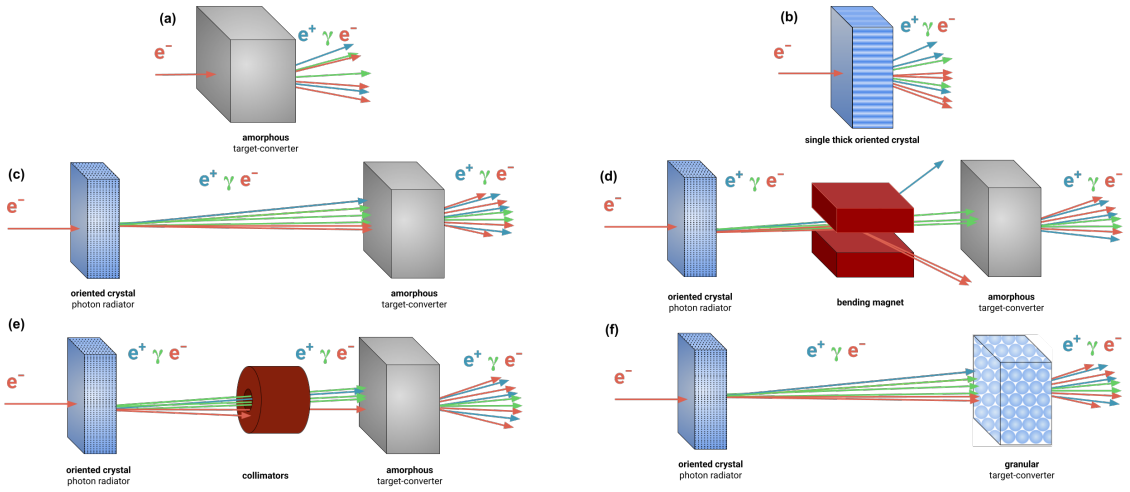


**Figure 1:** Schematic comparison of representative positron source configurations: **(a)** conventional source, **(b)** single thick oriented crystal, **(c)** basic hybrid scheme, **(d)** hybrid design with magnetic sweeping, **(e)** hybrid configuration with collimation, **(f)** granular converter concept.

New experimental campaigns at CERN, DESY, and MAMI have confirmed the feasibility of crystal-based positron sources across a range of materials and crystal thicknesses [20, 22, 23]. Proof-of-principle test at Orsay with 2 GeV electron beams demonstrated that thin (1–2 mm) crystals can produce intense photon fluxes while keeping thermal loads within acceptable limits [14]. Recent Baier–Katkov-based simulations [15, 24] suggest that even single-crystal configurations can operate safely at moderate intensities, offering a practical alternative to more complex hybrid setups.

## 3. Beam Tests and Experimental setups

Further beam tests have been conducted using similar experimental setups, which are schematized in Fig. 2. The setup was designed to enable precise crystal alignment, discriminate between photons and charged particles, and measure photon yields using a combination of tracking and calorimetry:

- **Particle identification:** threshold Čerenkov detectors upstream of the experimental setup detectors chain (not shown in Fig 2) to distinguish electrons and reject hadrons.
- **Upstream tracking:** two double-sided silicon microstrip planes ($9.3 \times 9.3$ cm$^2$ active area) placed $\sim 3$ m apart reconstruct the incident beam with $\sim 40$ $\mu$m spatial and 200 $\mu$rad angular resolution, including multiple scattering [25].
- **Crystal alignment:** the sample is held on a multi-axis goniometer with 5 $\mu$m translational and 1 $\mu$rad rotational precision, enabling sub-critical-angle alignment (~540 $\mu$rad).
- **Charged/neutral separation:** a 0.5-1.5 T·m dipole magnet downstream deflects charged secondaries while photons remain undeflected.
- **Active Photon Converter (APC):** a 0.1–0.4 $X_0$ Cu layer sandwiched between plastic scintillators; S0 (first one) vetoes primary charges and S1 (second one) records $e^+e^-$ pairs from photon conversions, providing a photon multiplicity monitor [20].
- **Calorimetry:** a 37 cm lead-glass electromagnetic calorimeter (24.6 $X_0$, $10 \times 10$ cm$^2$ area) measures total energy deposition. Calibration was performed with 1–6 GeV reference beams and verified via Monte Carlo simulation [26].

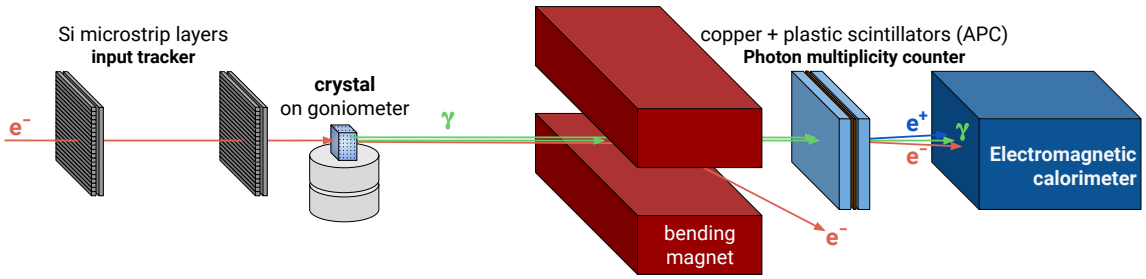


**Figure 2:** Schematic of the experimental setup: the electron beam (red) traverses the two silicon tracking detectors used for precise particle trajectory reconstruction. The crystalline sample is mounted on a high-precision goniometer to enable accurate alignment with respect to the beam axis. A dipole magnet spatially separates photons (green) from charged particles. The Active Photon Converter (APC) consists of a thin copper layer where incident photons are converted, producing electron-positron pairs (blue and red) which are subsequently detected. Finally, a lead glass calorimeter measures the total energy loss of each primary electron.

## 4. Results and simulation validation

### 4.1 Beam test results

Beam tests conducted at DESY (5.6 GeV) and CERN (6 GeV) using oriented W/Ir crystals demonstrate an increased count rate in the APC and an higher energy loss in axial alignment compared to random orientation. Comprehensive Monte Carlo simulations of the experiment were performed using the Geant4 [27–29] toolkit, incorporating the advanced `G4ChannelingFastSimModel`[1] [30, 31]. This model enables accurate simulation of coherent interactions within the crystalline medium integrating the quasiclassical Baier-Katkov formula along realistic particle trajectories [32, 33].

As shown in Fig. 3 the measured data exhibit good agreement with the Monte Carlo predictions that include both channeling and coherent radiation effects, thereby validating the robustness of the experimental setup and the fidelity of the simulation framework. The experimental results provided a benchmark for the simulation model, which was subsequently employed in the design and optimization of the FCC-ee positron source.

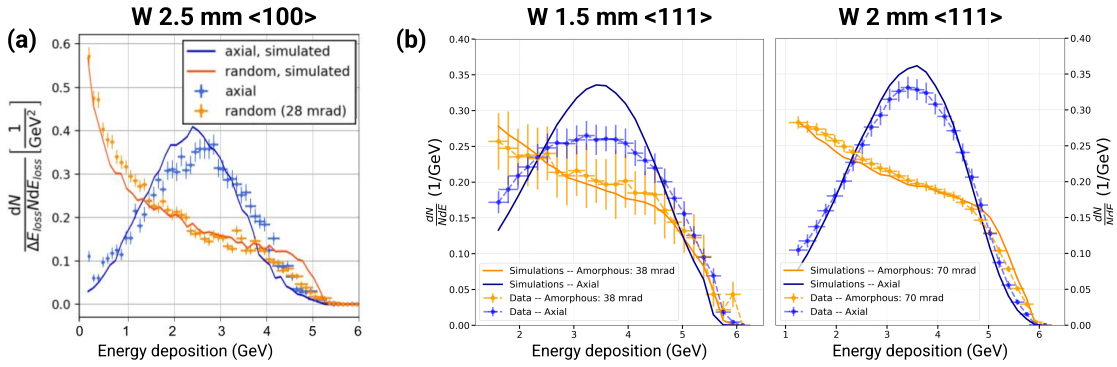


**Figure 3:** Experimental outcomes: (a) DESY results (5.6 GeV) adapted from [20], (b) CERN results (6 GeV) from [34].

### 4.2 Simulation of a crystal positron source for FCC-ee

Previous studies on crystalline positron source optimization have been conducted [22, 35], which focused on reducing the Peak Energy Deposition Density (PEDD), lowering the total energy deposited (Edep), and maximizing the positron yield by varying the target-to-collimator distance and by exploring collimators or magnetic elements. More recently, in [15], a combined simulation approach was adopted, using `G4ChannelingFastSimModel` for positron production and *RF-Track* [36] to model source performance in the positron capture system. Building on these works, a scan of the crystal thickness was performed to evaluate key metrics: accepted yield at the Damping Ring (DR), scaled primary bunch charge, PEDD, and deposited power. Optimal source performance is achieved for crystal thicknesses between 12 and 13 mm, where the accepted yield exceeds conventional schemes by about 10%, and deposited power is reduced by 14%. The PEDD

[1] Additional information about the Channeling Fast Sim Model can be found at G4ChannelingFastSimModel.

remains comparable to conventional values. The choice of a 12 mm tungsten crystal maximizes positron yield while reducing thermal load, as summarized in Table 1 and Figure 4. This optimization is an important contribution toward the development of practical positron sources for future high-luminosity colliders [15].

| Parameter | Conventional | Crystal-based |
|---|---|---|
| Target thickness [mm] | 15 | 12 |
| Production rate | 7.1 | 7.6 |
| Accepted yield at the DR | 3.03 | 3.36 |
| Primary bunch charge [nC] | 4.46 | 4.0 |
| Deposited power in the target [kW] | 1.14 | 0.98 |
| PEDD in the target [J/g/pulse] | 6.99 | 6.76 |

**Table 1:** Summary of FCC-ee positron source optimization results. From [15].

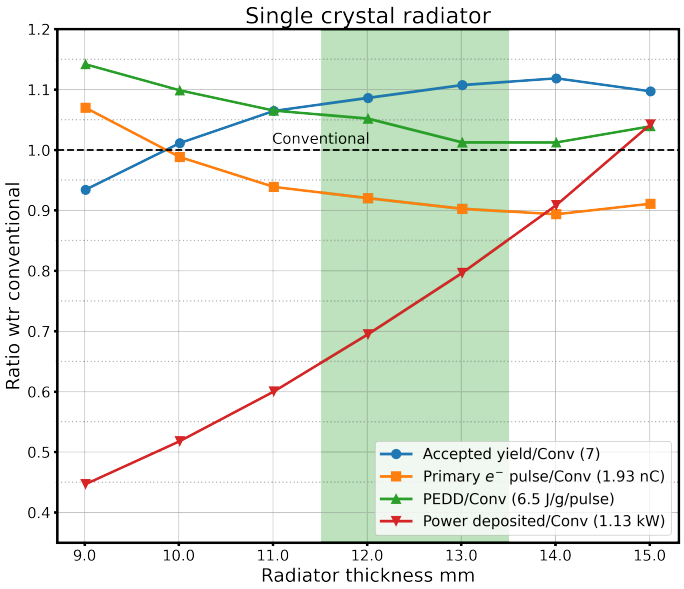


**Figure 4:** Simulation results for a single tungsten crystal at room temperature: accepted yield at the DR as a function of crystal thickness. The dashed line represents the simulation results for the conventional source, with conventional parameter values indicated in the legend. The green region highlights the optimal crystal thickness range (11.5–13.5 mm). Adapted from [15].

## 5. Future collider applications

Within the FCC-ee Injector Studies (WP3), crystal-based positron sources, both hybrid and single-crystal variants, are being benchmarked against conventional amorphous designs. Optimizations are driven by the validated simulation chain, with a forthcoming demonstrator scheduled within the CHART/PSI P3 program, including full capture-system integration [5].

## Acknowledgements

This research was supported by MUR PRIN (NRRP, NextGenerationEU) and conducted in collaboration with IJCLab (FCC-ee Injector Studies WP3) and CHART/PSI (P3).
We acknowledge financial support under the National Recovery and Resilience Plan (NRRP), Call for tender No. 104 published on 02.02.2022 by the Italian Ministry of University and Research (MUR), funded by the European Union – NextGenerationEU – Project Title : "Intense positron source Based On Oriented crySTals - e+BOOST" 2022Y87K7X – CUP I53D23001510006.

We gratefully acknowledge the beamtime provided by the test beam facility at DESY Hamburg (Germany), a member of the Helmholtz Association (HGF). We are also grateful to the CERN PS/SPS coordinators and the PS East Area T9 staff for their valuable support during the experimental setup phase. In particular, we are indebted to D. Banerjee and A. Ebn Rahmoun for their assistance.

This project has received funding from the European Union's Horizon Europe Research and Innovation programme under the EUROLABS project (G.A. 101057511).

We acknowledge ISCRA for awarding the project *IsCc7_ARCANE* access to the LEONARDO supercomputer, owned by the EuroHPC Joint Undertaking, hosted by CINECA (Italy).

This work was supported by the European Commission through the H2020-MSCA-RISE N-LIGHT (G.A. 872196), EIC-PATHFINDER-OPEN TECHNO-CLS (G.A. 101046458), MHz-TOMOSCOPY (G.A 101046448) and H2020-MSCA-IF-Global TRILLION (G.A.101032975) projects.

Iryna Chaikovska would like to thank the ANR (Agence Nationale de la Recherche) under Grant No. ANR-21-CE31-0007 for its support.

We also acknowledge partial support of INFN CSN1 (RD_FCC and RD_MUCOL projects) and CSN5 (OREO and Geant4INFN projects).

## Appendix: The e+BOOST Collaboration

L. Bandiera[a], S. Bertelli[b], D. Boccanfuso[c], S. Carsi, N. Canale[a,d], F. Cescato[a,d], D. De Salvador[e,f], P. Fedeli[a,d], V. Guidi[a,d], V. Haurylavets, A. O. M. Iorio[c], G. Lezzani[g,h], L. Malagutti[a], S. Mangiacavalli[g,h], A. Mazzolari[d], P. Monti-Guarnieri[i], R. Negrello[a,d], G. Paternò[a], L. Perna[l], S. Perna[c], M. Prest[g,h], M. Romagnoni[d], G. Saibene[g,h], A. Selmi[g,h], F. Sgarbossa[e,f], M. Soldani[m], A. Sytov[a], V.V. Tikhomirov, E. Vallazza[h], D. Valzani[e,f], G. Zuccalà[g,h]

[a] Istituto Nazionale di Fisica Nucleare, Sezione di Ferrara, Ferrara, Italy
[b] INFN Laboratori Nazionali di Frascati, Frascati, Italy
[c] Universita' di Napoli Federico II - INFN Napoli, Italy
[d] Dipartimento di Fisica e Scienze Della Terra, Università Degli Studi di Ferrara, Ferrara, Italy

[e] Dipartimento di Fisica e Astronomia, Università Degli Studi di Padova, Padua, Italy
[f] Istituto Nazionale di Fisica Nucleare, Laboratori Nazionali di Legnaro, Legnaro, Italy
[g] Università degli Studi dell'Insubria, Como, Italy
[h] INFN Sezione di Milano Bicocca, Milan, Italy
[i] Università degli Studi di Trieste, Trieste, Italy
[l] Gran Sasso Science Institute, INFN Laboratori Nazionali del Gran Sasso, L'Aquila, Italy
[m] CERN, Geneva, Switzerland

## References

[1] 2020 Update of the European Strategy for Particle Physics (Brochure), Tech. rep., Geneva (2020). doi:10.17181/CERN.JSC6.W89E.

[2] A. S. e. o. Abada A., Abbrescia M., Fcc-ee: The lepton collider, Eur. Phys. J. Spec. Top. 228, 261–623 (2019).

[3] M. Benedikt, et al., Future circular collider feasibility study report volume 2: Accelerators, technical infrastructure and safety, CERN accelerator reports, CERN-FCC-ACC-2025-0004doi:10.17181/CERN.EBAY.7W4X.

[4] S. Maloy, et al., Slc target analysis, Tech. Rep. LA-UR-01-1913, Los Alamos National Laboratory (Jun. 2001).

[5] P. Craievich, et al., Chart scientific report 2023: Fcc-ee injector study and the p3 project at psi, Tech. rep., CHART — Swiss Accelerator Research and Technology, Switzerland, accessed: 2025-10-23 (January 2024).
URL https://chart.ch/wp-content/uploads/2024/02/Report-2023-FCCee-Injector.pdf

[6] V. N. Baier, V. M. Katkov, V. M. Strakhovenko, Electromagnetic processes at high energies in oriented single crystals, 1998.

[7] W. Brandt, Channeling in crystals, Scientific American Magazine Vol. 218 No. 3 (1968).

[8] A. I. Akhiezer, N. F. Shulga, High-energy electrodynamics in matter, 1996.

[9] U. I. Uggerhøj, The interaction of relativistic particles with strong crystalline fields, Rev. Mod. Phys. 77 (2005) 1131–1171. doi:10.1103/RevModPhys.77.1131.

[10] J. Andersen, Channeling radiation and coherent bremsstrahlung, Nuclear Instruments and Methods 170 (1) (1980) 1–5. doi:https://doi.org/10.1016/0029-554X(80)90976-3.

[11] L. Bandiera, A. Sytov, D. De Salvador, A. Mazzolari, E. Bagli, R. Camattari, S. Carturan, C. Durighello, G. Germogli, V. Guidi, P. Klag, W. Lauth, G. Maggioni, V. Mascagna, M. Prest, M. Romagnoni, M. Soldani, V. Tikhomirov, E. Vallazza, Investigation on radiation generated by sub-gev electrons in ultrashort silicon and germanium bent crystals, Eur. Phys. J. C 81 (4),

cited by: 20; All Open Access, Gold Open Access, Green Open Access (2021). doi:10.1140/epjc/s10052-021-09071-2.

[12] R. Chehab, Positron sources (1989). doi:10.5170/CERN-1994-001.643.

[13] X. Artru, et al., Positron source using channeling in a tungsten crystal, Nucl. Instrum. Methods Phys. Res. A 344 (3) (1994) 443–454. doi:10.1016/0168-9002(94)90865-6.

[14] X. Artru, et al., Axial channeling of relativistic electrons in crystals as a source for positron production, Nucl. Instrum. Methods Phys. Res. B 119 (1) (1996) 246–252. doi:10.1016/0168-583X(96)00320-5.

[15] F. Alharthi, et al., Fcc-ee positron source from conventional to crystal-based, Nucl. Instrum. Methods Phys. Res. A 1075 (2025) 170412. doi:https://doi.org/10.1016/j.nima.2025.170412.

[16] R. Chehab, et al., Experimental study of a crystal positron source, Phys. Lett. B 525 (1) (2002) 41–48. doi:10.1016/S0370-2693(01)01395-8.

[17] R. Chehab, et al., Experiment with a crystal-assisted positron source using 6 and 10 gev electrons, Nucl. Instrum. Methods Phys. Res. B 201 (1) (2003) 243–252. doi:https://doi.org/10.1016/S0168-583X(02)01180-1.

[18] T. Suwada, et al., Measurement of positron production efficiency from a tungsten monocrystalline target using 4- and 8-gev electrons, Phys. Rev. E 67 (2003) 016502. doi:10.1103/PhysRevE.67.016502.

[19] S. Navas, et al., Review of particle physics, Physical review. D 110 (3) (8 2024). doi:10.1103/physrevd.110.030001.

[20] L. Bandiera, et al., Crystal-based pair production for a lepton collider positron source, Eur. Phys. J. C 82 (8) (aug 2022). doi:10.1140/epjc/s10052-022-10666-6.

[21] I. Chaikovska, et al., Positron sources: from conventional to advanced accelerator concepts-based colliders, J. Instrum. 17 (05) (2022) P05015. doi:10.1088/1748-0221/17/05/P05015.

[22] M. Soldani, et al., Radiation in oriented crystals: Innovative application to future positron sources, Nucl. Instrum. Methods Phys. Res. A 1058 (2024) 168828. doi:10.1016/j.nima.2023.168828.

[23] H. Shen, et al., Channeling and radiation of 855 MeV electrons and positrons in straight and bent tungsten (1 1 0) crystals, Nucl. Instrum. Methods Phys. Res. B 424 (2018) 26–36. doi:10.1016/j.nimb.2018.03.025.

[24] V. Baier, et al., Electromagnetic Processes At High Energies In Oriented Single Crystals, World Scientific Publishing Company, 1998. doi:https://books.google.it/books?id=18TsCgAAQBAJ.

[25] M. Prest, et al., The AGILE silicon tracker: an innovative gamma-ray instrument for space, Nucl. Instrum. Methods Phys. Res. A 501 (1) (2003) 280–287. doi:10.1016/s0168-9002(02)02047-8.

[26] F. Ambrosino, et al., The large-angle photon veto system for the NA62 experiment at CERN, IEEE Nucl. Sci. Symp. (2011). doi:10.1109/nssmic.2011.6154594.

[27] S. Agostinelli, et al., Geant4—a simulation toolkit, Nucl. Instrum. Methods Phys. Res. A 506 (3) (2003) 250–303. doi:10.1016/S0168-9002(03)01368-8.

[28] J. Allison, et al., Recent developments in Geant4, Nucl. Instrum. Methods Phys. Res. A 835 (2016) 186–225. doi:10.1016/j.nima.2016.06.125.

[29] J. Allison, et al., Geant4 developments and applications, IEEE Trans. Nucl. Sci. 53 (1) (2006) 270–278. doi:10.1109/tns.2006.869826.

[30] A. Sytov, et al., Simulation code for modeling of coherent effects of radiation generation in oriented crystals, Phys. Rev. Accel. Beams 22 (2019) 064601. doi:10.1103/PhysRevAccelBeams.22.064601.

[31] A. Sytov, et al., Geant4 simulation model of electromagnetic processes in oriented crystals for accelerator physics., J. Korean Phys. Soc. 83 (2) (2023) 132–139. doi:10.1007/s40042-023-00834-6.

[32] L. Bandiera, et al., RADCHARM++: A C++ routine to compute the electromagnetic radiation generated by relativistic charged particles in crystals and complex structures, Nucl. Instrum. Methods Phys. Res. B 355 (2015) 44–48. doi:10.1016/j.nimb.2015.03.031.

[33] L. Bandiera, et al., Strong reduction of the effective radiation length in an axially oriented scintillator crystal, Phys. Rev. Lett. 121 (2018) 021603. doi:10.1103/PhysRevLett.121.021603.

[34] N. Canale, M. Romagnoni, A. Sytov, et al., Coherent radiation in axially oriented industrial-grade tungsten crystals: A viable path for an innovative $\gamma$-rays and positron sources, Nucl. Instrum. Methods Phys. Res. A 1075 (2025) 170342. doi:https://doi.org/10.1016/j.nima.2025.170342.

[35] D. Boccanfuso, et al., Study of a high intensity positron source based on oriented crystals, Il Nuovo Cimento C (2025). doi:10.1393/ncc/i2025-25108-0.

[36] A. Latina, Rf-track reference manual (Jun. 2020). doi:10.5281/zenodo.3887085.
URL https://doi.org/10.5281/zenodo.3887085